



Deep nightside photoelectron observations by MAVEN SWEA: Implications for Martian northern hemispheric magnetic topology and nightside ionosphere source

Shaosui Xu, David Mitchell, Michael Liemohn, Chuanfei Dong, Stephen Bougher,
Matthew Fillingim, Robert Lillis, James Mcfadden, Christian Mazelle, Jack
Connerney, et al.

► To cite this version:

Shaosui Xu, David Mitchell, Michael Liemohn, Chuanfei Dong, Stephen Bougher, et al.. Deep nightside photoelectron observations by MAVEN SWEA: Implications for Martian northern hemispheric magnetic topology and nightside ionosphere source. *Geophysical Research Letters*, 2016, 43, pp.8876-8884. <10.1002/2016GL070527>. <insu-03669435>

HAL Id: insu-03669435

<https://insu.hal.science/insu-03669435v1>

Submitted on 17 May 2022

HAL is a multi-disciplinary open access archive for the deposit and dissemination of scientific research documents, whether they are published or not. The documents may come from teaching and research institutions in France or abroad, or from public or private research centers.

L'archive ouverte pluridisciplinaire **HAL**, est destinée au dépôt et à la diffusion de documents scientifiques de niveau recherche, publiés ou non, émanant des établissements d'enseignement et de recherche français ou étrangers, des laboratoires publics ou privés.



Copyright - All rights reserved

RESEARCH LETTER

10.1002/2016GL070527

Key Points:

- MAVEN SWEA instrument observed photoelectrons at altitudes below 200 km in deep nightside
- It suggests the presence of large cross-terminator closed crustal magnetic field loops over the Martian northern hemisphere
- Such topologies also provide new energy sources to the nightside ionosphere

Correspondence to:

S. Xu,
shaosui.xu@ssl.berkeley.edu

Citation:

Xu, S., et al. (2016), Deep nightside photoelectron observations by MAVEN SWEA: Implications for Martian northern hemispheric magnetic topology and nightside ionosphere source, *Geophys. Res. Lett.*, 43, 8876–8884, doi:10.1002/2016GL070527.

Received 20 JUL 2016

Accepted 20 AUG 2016

Accepted article online 25 AUG 2016

Published online 10 SEP 2016

Deep nightside photoelectron observations by MAVEN SWEA: Implications for Martian northern hemispheric magnetic topology and nightside ionosphere source

Shaosui Xu^{1,2}, David Mitchell¹, Michael Liemohn², Chuanfei Dong^{2,3}, Stephen Bougher², Matthew Fillingim¹, Robert Lillis¹, James McFadden¹, Christian Mazelle⁴, Jack Connerney⁵, and Bruce Jakosky⁶

¹Space Sciences Laboratory, University of California, Berkeley, California, USA, ²Department of Climate and Space Sciences and Engineering, University of Michigan, Ann Arbor, Michigan, USA, ³Department of Astrophysical Sciences and Princeton Plasma Physics Laboratory, Princeton University, Princeton, New Jersey, USA, ⁴IRAP, CNRS and University Paul Sabatier, Toulouse, France, ⁵GSFC, Greenbelt, Maryland, USA, ⁶LASP, University of Colorado, Boulder, Colorado, USA

Abstract The Mars Atmosphere and Volatile Evolution (MAVEN) mission samples the Mars ionosphere down to altitudes of ~150 km over a wide range of local times and solar zenith angles. On 5 January 2015 (Orbit 520) when the spacecraft was in darkness at high northern latitudes (solar zenith angle, SZA > 120°; latitude > 60°), the Solar Wind Electron Analyzer (SWEA) instrument observed photoelectrons at altitudes below 200 km. Such observations imply the presence of closed crustal magnetic field loops that cross the terminator and extend thousands of kilometers to the deep nightside. This occurs over the weak northern crustal magnetic source regions, where the magnetic field has been thought to be dominated by draped interplanetary magnetic fields (IMF). Such a day-night magnetic connectivity also provides a source of plasma and energy to the deep nightside. Simulations with the SuperThermal Electron Transport (STET) model show that photoelectron fluxes measured by SWEA precipitating onto the nightside atmosphere provide a source of ionization that can account for the O₂⁺ density measured by the Suprathermal and Thermal Ion Composition (STATIC) instrument below 200 km. This finding indicates another channel for Martian energy redistribution to the deep nightside and consequently localized ionosphere patches and potentially aurora.

1. Introduction

At Mars, superthermal electrons, of both ionospheric and solar wind origin, are excellent tracers of magnetic topology [e.g., Mitchell et al., 2001; Liemohn et al., 2006a; Brain et al., 2007; Xu et al., 2014] and are also an important energy source in the nightside ionosphere [e.g., Fox et al., 1993]. Martian crustal magnetic anomalies influence the interaction between solar wind and the Martian plasma environment, resulting in a complex magnetic topology [e.g., Brain et al., 2003; Harnett and Winglee, 2005; Liemohn et al., 2006b, 2007; Ma et al., 2014]. In the Martian environment, superthermal electrons often gyrate around and follow the magnetic field line, obeying the first adiabatic invariant. However, significant pitch angle scattering occurs in some of the Martian environment where there are either sizable magnetic fluctuations, such as in the magnetosheath, or considerable collisions with atmospheric species, such as below altitude ~200 km. In addition, near the strong crustal sources, drift motion across the magnetic field lines can be important [e.g., Harada et al., 2016]. Electrons' energy distributions can infer the origins of these electrons, e.g., ionospheric or solar wind [Mitchell et al., 2001]. Therefore, determining the plasma source regions on a field line via pitch angle-resolved energy spectra is a reliable way to deduce the magnetic topology. For example, Brain et al. [2007] determined whether a field line is closed or open (or draped) by analyzing the electron angular distribution measured by the magnetometer/electron reflectometer [Acuña et al., 1992; Mitchell et al., 2001] on board the Mars Global Surveyor (MGS) spacecraft [Acuña et al., 1998]. Studies [e.g., Liemohn et al., 2006a; Frahm et al., 2006; Coates et al., 2011] have also identified photoelectron samples in the high-altitude Martian tail with measurements from the Analyzer of Space Plasma and Energetic Atoms (ASPERA-3) experiment [Barabash et al., 2006] onboard the Mars Express spacecraft. Liemohn et al. [2006b] then suggested that direct magnetic connectivity to the dayside ionosphere can explain these high-altitude photoelectron observations in the tail. Such photoelectron observations in the tail were then used to estimate ambipolar electric field-driven photoelectron escape at Mars

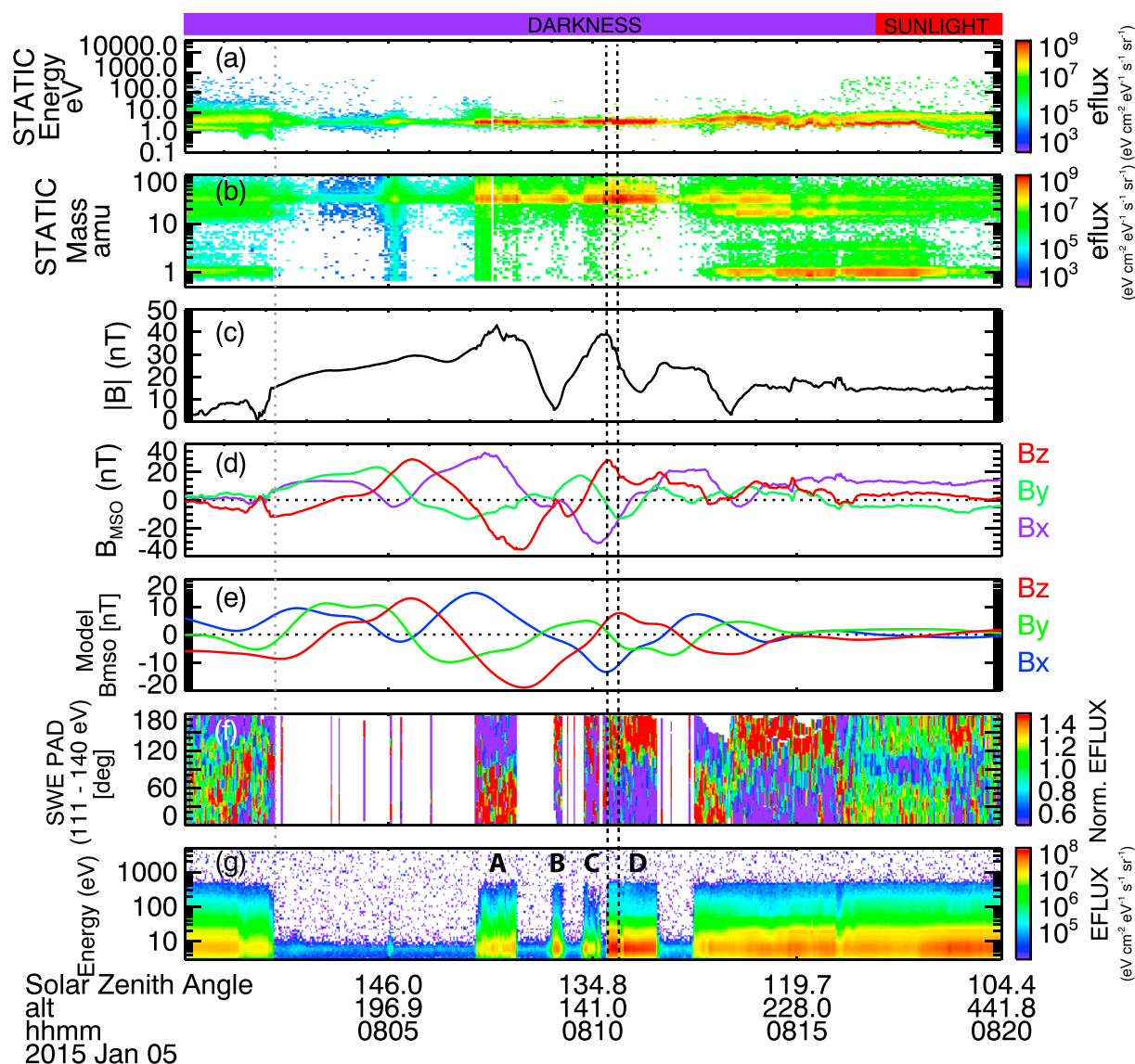


Figure 1. A MAVEN orbit example (Orbit 520) begins at universal time (UT) 08:00:00 5 January 2015. (a–g) Time series of STATIC ion energy spectrum, STATIC ion mass spectrum, MAG magnetic field magnitude and components in MSO coordinates, model magnetic field in MSO coordinates, SWEA normalized electron pitch angle distribution (111.2–140.3 eV), and SWEA electron energy spectrum. The bar on the top shows when the spacecraft is in sunlight (red) and in darkness (purple). Both electron and ion energy fluxes are in units of $\text{eV s}^{-1} \text{cm}^{-2} \text{sr}^{-1} \text{eV}^{-1}$. The dotted gray vertical line indicates where the electron voids start and the two vertical dashed lines mark the time period, over which electron energy spectra shown in Figure 2 (right) are averaged. Four electron patches are labeled as A, B, C, and D in Figure 1g.

[Frahm et al., 2010], Venus [Coates et al., 2015], and Titan [Coates et al., 2012]. The Martian nightside ionosphere is known to have low densities and be quite patchy [e.g., Gurnett et al., 2008; Němec et al., 2010]. Precipitation of superthermal electrons into the nightside atmosphere should cause ionization [e.g., Lillis et al., 2009; Fillingim et al., 2007, 2010] and possibly auroral emissions [e.g., Haider et al., 1992; Seth et al., 2002; Brain et al., 2006a] in localized regions.

However, on the Martian nightside, no in situ observation had been made below 250 km altitude (the periapasis of Mars Express) until the Mars Atmosphere and Volatile Evolution (MAVEN) mission [Jakosky et al., 2015]. From December 2014 to February 2015, MAVEN's periapasis was on the nightside at high northern latitudes, where crustal magnetic fields are generally much weaker than those in the south [e.g., Connerney et al., 2005]. In particular, over two large regions, Utopia Planitia and the Tharsis rise, the observed magnetic field at 400 km MGS altitude is thought to be dominated by fields induced by the solar wind interaction, although the

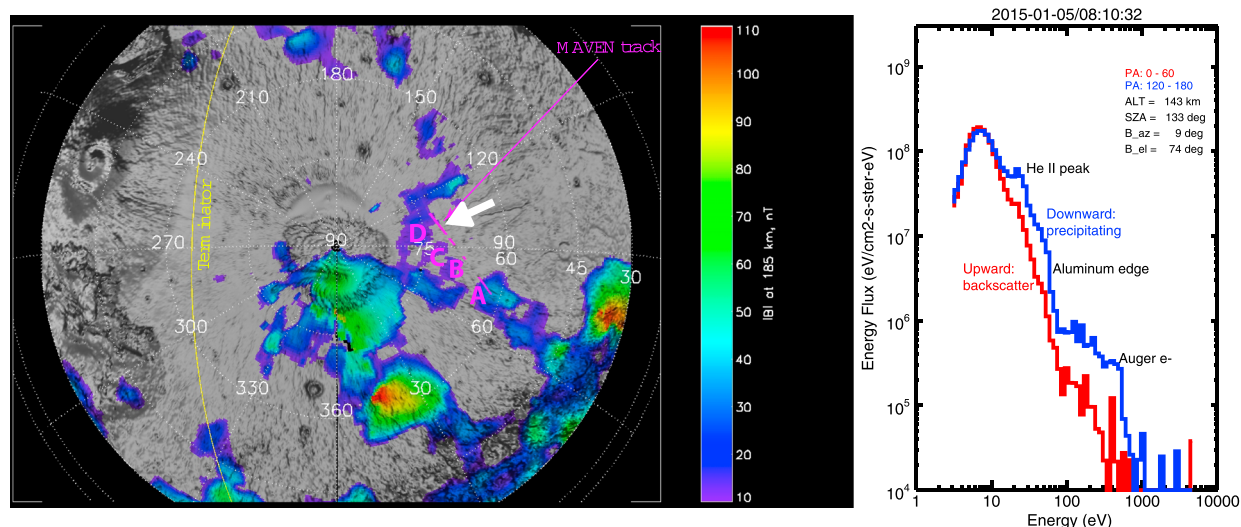


Figure 2. (left) The orbit track of the four patches A, B, C, and D in Figure 1 in pink superimposed on a map of crustal magnetic field magnitude at 185 km altitude derived from electron reflection magnetometry and published by *Lillis et al.* [2008b]. The terminator is shown in yellow. (right) An averaged electron energy spectra centered at UT 08:10:32 5 January 2015, as indicated by the dashed vertical lines in Figure 1 and also the white arrow in Figure 2. The red line is for pitch angle 0–60° and the blue line for pitch angle 120°–180°. The altitude in kilometers, solar zenith angle and magnetic azimuthal and elevation angles in degree of this electron measurement are shown at the upper right corner.

draping pattern is asymmetric and may be influenced by the presence of crustal sources far from the spacecraft [Brain et al., 2006b]. The MAVEN mission provides a comprehensive set of plasma and magnetic field observations to altitudes as low as ~150 km (~120 km during “deep dips”) and allows us to reexamine the current understanding of the Martian northern hemisphere. Here we report measurements of ionospheric primary photoelectrons obtained with the MAVEN Solar Wind Electron Analyzer (SWEA) [Mitchell et al., 2016] at high solar zenith angles (> 120°) and low altitudes (< 200 km). The presence of ionospheric photoelectrons below the exobase in darkness has important implications for the low-altitude Martian magnetic topology (section 3) and also for energy transport to the nightside ionosphere (section 4).

2. Deep Nightside Low-Altitude Photoelectron Observations

Part of MAVEN Orbit 520 is shown in Figure 1. From Figures 1a to 1g, the panels show ion energy spectrum and ion mass spectrum measured by the Suprathermal and Thermal Ion Composition (STATIC) [McFadden et al., 2015], magnetic field magnitude and three components measured by the Magnetometer (MAG) [Connerney et al., 2015] in Mars-centered Solar Orbital (MSO) coordinates, modeled magnetic field in MSO coordinates [Morschhauser et al., 2014], normalized electron pitch angle distribution (111.2–140.3 eV), and electron energy spectrum measured by SWEA [Mitchell et al., 2016], against time. The bar on the top shows whether the spacecraft is in sunlight (red) or in darkness (purple). Soon after 08:02 UT (universal time, as indicated by the dotted gray vertical line), the SWEA measurement shows a superthermal electron depletion (also called electron void) that lasts for about 5 min, which is thought to be associated with localized closed crustal magnetic field loops, with both foot points in darkness [e.g., Steckiewicz et al., 2015]. These closed loops exclude external sources of plasma (from the solar wind or dayside ionosphere), while any electrons trapped on the loops are either lost or degraded in energy below SWEA’s measurement threshold mainly by collisions with the neutral atmosphere.

From 08:05 to 08:14 UT, when the spacecraft dips below ~ 200 km, we observe four isolated, sharply defined regions (labeled as A, B, C, and D) where the superthermal electron flux is orders of magnitude higher than within the electron voids. The orbit tracks of these four patches are shown in Figure 2 (left). The extents of these regions range from ~100 to ~300 km along the spacecraft trajectory (mostly horizontal near periapsis). In particular, unmistakable photoelectron signatures are seen for the time range 08:10–08:12 UT. To demonstrate, Figure 2 (right) is an example of electron energy spectra averaged over the time period indicated by the two vertical lines in Figure 1. The spacecraft was at altitude 143 km in deep nightside (SZA ~ 133°), red for pitch angle (PA) 0–60° and the blue line for PA 120°–180°. The magnetic elevation angle, or the angle between the

local magnetic field direction and the horizontal plane, is 74° . For PA $120^\circ - 180^\circ$ (blue line), i.e., electrons traveling toward the planet, typical photoelectron features can be identified, including the enhancement from 20 to 30 eV due to the ionization of CO_2 and O by the intense solar He II emission line at 30.4 nm and also the sharp decrease of the electron flux (the Aluminum edge) near 50–70 eV caused by the sudden drop in solar EUV flux below 15 nm, as well as the Auger (inner shell) electrons near 500 eV due to X-ray ionization [e.g., Mantas and Hanson, 1979; Mitchell et al., 2000; Liemohn et al., 2003]. For PA $0^\circ - 60^\circ$ (red line, traveling away from the planet), the spectrum is generally the same shape, including the He II peak and the sharp drop near 60 eV but with rather low fluxes at high energies. The differences in spectral shape might be explained if the upward traveling electron population is derived from the downward traveling population after it has been magnetically reflected and backscattered. We will describe this hypothesis in more detail below.

3. Interpretation of Nightside Photoelectron Observations

How can photoelectrons produced on the sunlit hemisphere be observed below 200 km altitude in the night hemisphere thousands of kilometers away from the terminator? They cannot be transported from the day-side at altitudes below 200 km (i.e., horizontal flow through the ionosphere) because collisions with the atmospheric neutral particles and thermal plasma would cause significant depletion, as indicated by the surrounding electron depletion regions on either side of these patches. For the same reason, photoelectrons cannot be carried to these locations in the night hemisphere by the planet's rotation, especially without double-loss cone distributions present. The most prominent region of nightside photoelectrons (Figure 1g, patch D) exhibits fluxes comparable to values in the sunlit ionosphere at 100° solar zenith angle (08:20 UT), suggesting little, if any, attenuation along the path traveled. Electron pitch angle distributions during this interval (Figure 1) show a much higher flux for electrons traveling antiparallel to the magnetic field than for electrons traveling in the opposite direction. This pattern indicates transport of photoelectrons from the day-side ionosphere and precipitation onto the nightside atmosphere. Note that the MSO X component of the magnetic field is negative at the beginning of patch D (Figure 1), indicating that photoelectrons produced on the dayside are observed on the nightside with a component of motion toward the Sun. At face value this seems counterintuitive; however, there is a significant rotation of the magnetic field over patch D during which the superthermal electron flux remains antiparallel to field direction. This suggests a localized twist or kink in the field and highlights the risk of inferring magnetic field topology from the field direction alone. For all four patches examined here, we infer that the deep Martian nightside is magnetically connected to the sunlit hemisphere.

The magnetic configuration that connects the sunlit ionosphere with the low-altitude (< 200 km) nightside atmosphere is unlikely to be a draped magnetic field line, which tends to flare away from the planet downstream of the terminator. On the contrary, photoelectrons are observed on the nightside at an altitude of 143 km and on a field line directed away from the planet, with a magnetic elevation angle of 74° . A more reasonable magnetic configuration would be a closed crustal magnetic field line that straddles the terminator. Studies with the SuperThermal Electron Transport (STET) model [Liemohn et al., 2003; Xu and Liemohn, 2015] have shown that semivertical transport of photoelectrons along a magnetic field line can take place without significant flux decrease above the superthermal electron exobase or the altitude above which collisions between superthermal electrons and atmospheric species become negligible. This altitude varies with electron energy (because of the collision cross section) and also depends on the atmospheric density profile. It is generally in the altitude range from 130 to 170 km [e.g., Mantas and Hanson, 1979; Lillis et al., 2008a; Xu et al., 2015a; Steckiewicz et al., 2015; Xu et al., 2016]. In other words, the magnetic field must rise above the electron exobase between the night hemisphere, where photoelectrons are observed, and the source region in the dayside ionosphere, thus avoiding significant attenuation in transit.

Such magnetic configurations are present in simulations with the Block-Adaptive Tree Solarwind Roe-type Upwind Scheme (BATS-R-US) Mars multifluid Magnetohydrodynamics (MF-MHD) model [Najib et al., 2011; Dong et al., 2014]. The MF-MHD model solves the continuity, momentum, and energy equations separately for four ion fluids: H^+ , O^+ , O_2^+ , and CO_2^+ . An example of MF-MHD simulations with solar maximum (an Earth $F_{10.7} = 200$ solar flux unit, sfu) and perihelion conditions, case 17 of Dong et al. [2015], shows that closed magnetic loops extend thousands of kilometers, connecting crustal sources on either side of the terminator, as illustrated in Figure 3. Photoelectrons are produced on the dayside ionosphere (Figure 3, white arrows) then travel along magnetic field lines above the electron exobase and finally precipitate into the nightside ionosphere. The relative variations of the vector components of the model magnetic field (Figure 1e) are very

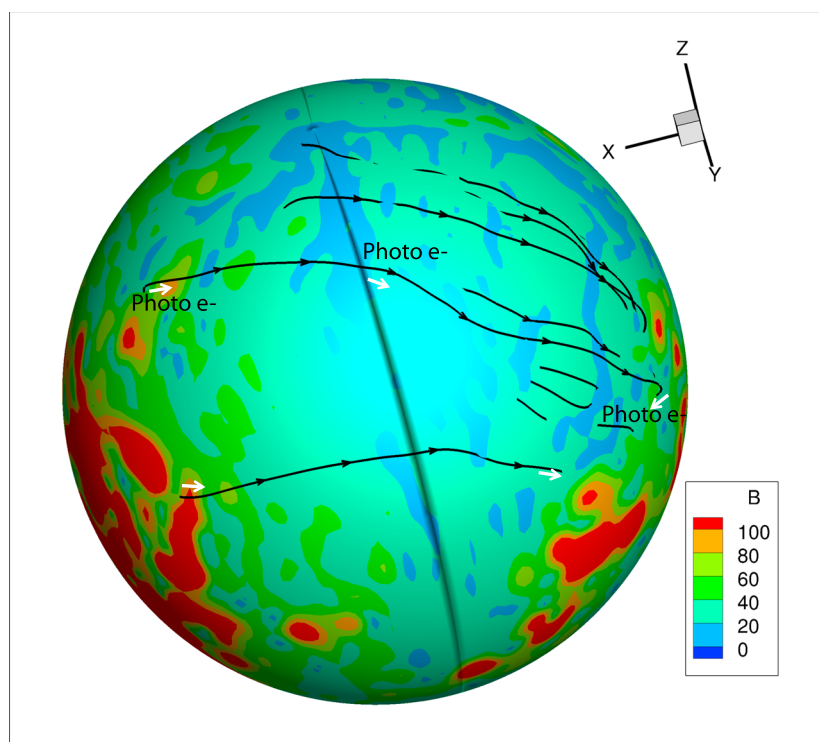


Figure 3. Magnetic strength and several magnetic field lines from a Mars multifluid MHD simulation with solar maximum and perihelion conditions. The magnetic field strength (nT) at 170 km altitude is shown in color. The white arrows indicate photoelectrons flowing along magnetic field from sunlit region to deep nightside. The black arrows show the direction of the magnetic fields.

similar to the observed variations (Figure 1d), although the amplitudes are different. This suggests a crustal origin for the observed field, modified by the solar wind interaction, as opposed to a draped interplanetary magnetic field (IMF). This further supports our interpretation of the magnetic field configuration during this observation.

4. Ion Observations and Production by Photoelectrons

The precipitation of photoelectrons into the deep nightside provides a localized but continuous particle and energy supply as long as there is magnetic connectivity to the dayside ionosphere. Since the precipitating electrons have sufficient energy to cause impact ionization, they should produce a localized ionospheric patch on the nightside. In fact, planetary ions (primarily O_2^+) are observed at the same times that precipitating photoelectrons are present (Figure 1, 08:07 to 08:12 UT). The boundaries separating regions of superthermal electron precipitation and voids are more sharply defined than the corresponding patches of O_2^+ ions, at least in part because the ion-neutral collision frequency is much higher than the electron-neutral collision frequency so that below 200 km the ions are more diffusive than electrons. From 08:02 to 08:12 UT, STATIC measures an ion population peaked at a mass of 32 amu and at an energy of 3 eV due to the spacecraft orbital velocity of 4.2 km/s. The mass peak extends from 25 amu to 40 amu and therefore can include variety species that STATIC cannot differentiate. In the dayside Mars' atmosphere, these ions are certain to be dominated by O_2^+ . However, on the nightside, other long-lived ion species, such as NO^+ , might be important [González-Galindo *et al.*, 2013]. However, for convenience, the mass range of 25 – 40 amu is referred as " O_2^+ " hereafter.

We considered three possible mechanisms that might be responsible for such a nightside ionosphere: the bulk thermal plasma transport from dayside to night, ion transport along the crustal magnetic loop, possibly aided by ambipolar electric fields, and local production by electron impact ionization. Both transport mechanisms are unlikely because O_2^+ ions are observed at altitudes as low as 143 km, a region that is inaccessible to transport because of collisions with neutral atmospheric species. Thus, we focus our attention on local

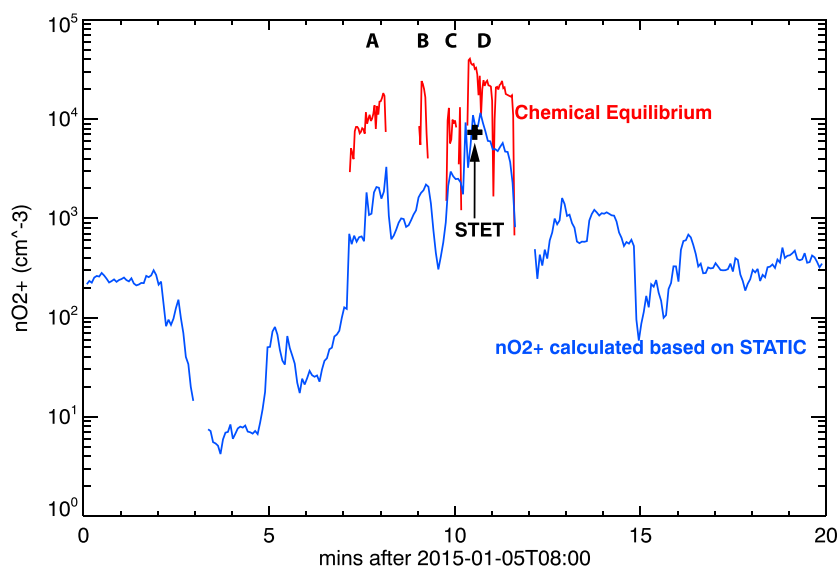


Figure 4. Observed O_2^+ density by STATIC of Orbit 520 (blue) and calculated O_2^+ density due to photoelectron impact ionization (red) as a function of time. The four red segments correspond to the four electron patches in Figure 1. The black cross illustrates the modeled O_2^+ density with the STET model.

production by electron impact ionization, which should mainly produce O_2^+ because the main neutral species is CO_2 at low altitudes.

The first step is to ionize CO_2 through electron impact ionization. The resulting CO_2^+ ions are then rapidly converted to O_2^+ through rapid chemical reactions. Assuming chemical equilibrium and ion production is balanced by recombination, the electron density, $n_e(z)$, is

$$n_e(z) = (P(z)/\alpha_{\text{eff}}(z))^{0.5} \quad (1)$$

where z is altitude, $P(z)$ is the ion production rate and $\alpha_{\text{eff}}(z)$ is the effective recombination rate. Because of the fast chemical reactions between CO_2 and O , $\alpha_{\text{eff}}(z)$ is well approximated by the dissociative recombination rate of O_2^+ [e.g., Sheehan and St-Maurice, 2004]:

$$\alpha_{\text{eff}}(z) = 1.95 \times 10^{-7} (300/T_e(z))^{0.7} \quad (2)$$

where $T_e(z)$ is the electron temperature. Assuming charge neutrality, we can replace $n_e(z)$ in equation (1) with O_2^+ density. We calculate the ion production rate, $P(z)$, from the measured superthermal electron flux precipitating into a model atmosphere based on the Mars Global Ionosphere-Thermosphere Model (M-GITM) [Bougher et al., 2015]. The neutral profiles and the electron temperature profile used are at latitude 67.5° and local midnight from a M-GITM run at solar longitude 270° and driven by an EUV flux corresponding to an Earth $F_{10.7}$ of 130 sfu. Even though M-GITM does not simulate the ionosphere past SZA 105, the nightside electron temperature is obtained from an empirical formula provided by Fox [1993]. This approximation is appropriate as we focus on low-altitude calculations, where electron and neutral temperatures are not substantially different. The ion production rate is the product of the superthermal electron flux, impact ionization cross section, and CO_2 density.

The calculated O_2^+ density is shown by the red line in Figure 4 for 08:03–08:12 UT, and the observed ion density based on mass 25–40 amu is shown in blue. The observed and calculated O_2^+ densities have similar profiles. The calculated O_2^+ density due to the electron impact ionization is comparable to or higher than the density determined from STATIC measurements, which demonstrates that the measured precipitating electron flux can account for the observed O_2^+ population.

On the other hand, between 08:07 and 08:12 UT, the calculated ion density is about an order of magnitude higher than the observations. This is likely because our simple calculation assumes that the measured superthermal electron flux produces ionization only locally, instead of over an altitude range. A more accurate (and computationally expensive) calculation was performed with the STET model, which solves the

gyro-averaged Boltzman equation and calculates the superthermal electron flux distribution along a single magnetic field line (see model details in Xu and Liemohn [2015] and Xu et al. [2015b]). The run was initialized with an upper boundary distribution at an altitude of 143 km set to the measured downward superthermal electron flux (as shown in Figure 2, right) and using the same neutral density and electron and ion temperature profiles from the aforementioned M-GITM simulation. We assume a negligible thermal plasma density (10^{-11} times the atomic oxygen density) to isolate the effects of ionization by precipitating superthermal electrons. We seek to determine whether the observed precipitating electron flux can account for the measured ion density at the same location. The model then calculates the superthermal electron flux over the entire field line so that we can calculate the ion production rate along the line. The modeled ion production at 143 km altitude is marked as the black cross in Figure 4, which matches well with the observed density from STATIC. The density from our more accurate STET calculation is about 1 order of magnitude lower than the simple calculation with equations (1) and (2) (red line), because in the STET simulation, ions are produced over a 10 km altitude range.

5. Conclusions and Future Work

We have presented observations of ionospheric primary photoelectrons that were obtained in darkness at high northern latitudes, where crustal magnetic sources are weak, and at altitudes below the electron exobase. The presence of photoelectrons at this location cannot be explained by horizontal, low-altitude transport over distances of 1400–2100 km because of collisions with atmospheric neutrals. Instead, these electrons must be transported at altitudes above the electron exobase along magnetic field lines with one footprint in the sunlit ionosphere (the source region) and the other footprint at low altitudes on the night hemisphere. The large magnetic elevation (74°) at the observation altitude of 140 km strongly suggests that the field line is a closed crustal magnetic loop that connects distant magnetic source regions. Such field lines are present in MHD simulations. This is contrary to the conventional view that ionospheric magnetic fields in the northern hemisphere are dominated by the draped IMF, as inferred from MGS observations at higher altitudes [Brain et al., 2007]. This suggests the presence of a low-altitude region of closed crustal magnetic loops underlying the draped IMF at higher altitudes. Photoelectrons this deep on the nightside so far have not been identified in the MGS electron data. This would be consistent with a transition to a predominantly draped IMF configuration, which MGS sampled at ~ 400 km altitude.

Magnetic connectivity to the dayside ionosphere also provides a source of energy and ionization to the Martian nightside atmosphere. Both chemical equilibrium calculations and more sophisticated simulations with the STET model demonstrate that the measured precipitating electron flux can support the observed O_2^+ density through electron impact ionization. Thus, magnetic connection to the dayside ionosphere could account for some of the nightside ionospheric patches inferred from radio occultation and radar sounding observations [Zhang et al., 1990; Gurnett et al., 2008; Duru et al., 2011].

From the preliminary examination of hundreds of orbits, such nightside precipitation of photoelectrons is quite common. The next step of this study is to conduct a statistical study of nightside and low-altitude photoelectron observations and characterize the occurrence rate by different parameters, such as solar zenith angle, magnetic configuration, and the upstream conditions. Furthermore, a similar study can be done in the southern hemisphere as MAVEN's periapsis precesses. With such a global view, energy input due to photoelectrons, an important channel for energy redistribution at Mars, to the nightside can be quantified. Consequently, we can also estimate how much of nightside ionosphere (below 200 km) is controlled by the intrinsic crustal fields, both depletion and photoelectron precipitation, as opposed to solar wind precipitation.

References

- Acuña, M., et al. (1992), Mars observer magnetic fields investigation, *J. Geophys. Res.*, 97(E5), 7799–7814.
- Acuña, M., et al. (1998), Magnetic field and plasma observations at Mars: Initial results of the Mars global surveyor mission, *Science*, 279(5357), 1676–1680.
- Barabash, S., et al. (2006), The Analyzer of Space Plasmas and Energetic Atoms (ASPERA-3) for the Mars Express mission, *Space Sci. Rev.*, 126(1–4), 113–164.
- Bougher, S., D. Pawlowski, J. Bell, S. Nelli, T. McDunn, J. Murphy, M. Chizek, and A. Ridley (2015), Mars global ionosphere-thermosphere model: Solar cycle, seasonal, and diurnal variations of the Mars upper atmosphere, *J. Geophys. Res. Planets*, 120, 311–342, doi:10.1002/2014JE004715.
- Brain, D., F. Bagenal, M. Acuña, and J. Connerney (2003), Martian magnetic morphology: Contributions from the solar wind and crust, *J. Geophys. Res.*, 108(A12), 1424, doi:10.1029/2002JA009482.

Acknowledgments

The authors would like to thank NASA and NSF for their support of this project under grants NNX13AG26G and AST-0908311. This work was also supported by the NASA Mars Scout Program. The authors thank the Rackham graduate school of University of Michigan for the research grant that supports S. Xu's visit at SSL, University of California, Berkeley, which makes this study possible. C.F. Dong is supported by the NASA Living With a Star Jack Eddy Postdoctoral Fellowship Program, administered by the University Corporation for Atmospheric Research. The MAVEN data used in this study are available through Planetary Data System. The BATS-R-US code is publicly available from <http://csem.engin.umich.edu/tools/swmf>. For distribution of the model results used in this study, please contact C. Dong (dcfy@pppl.gov).

- Brain, D., J. Halekas, L. Peticolas, R. Lin, J. Luhmann, D. Mitchell, G. Delory, S. Bougher, M. Acuña, and H. Rème (2006a), On the origin of aurora on Mars, *Geophys. Res. Lett.*, **33**, L01201, doi:10.1029/2005GL024782.
- Brain, D., R. Lillis, D. Mitchell, J. Halekas, and R. Lin (2007), Electron pitch angle distributions as indicators of magnetic field topology near Mars, *J. Geophys. Res.*, **112**, A09201, doi:10.1029/2007JA012435.
- Brain, D. A., D. L. Mitchell, and J. S. Halekas (2006b), The magnetic field draping direction at Mars from April 1999 through August 2004, *Icarus*, **182**(2), 464–473.
- Coates, A. J., S. Tsang, A. Wellbrock, R. Frahm, J. Winningham, S. Barabash, R. Lundin, D. Young, and F. Crary (2011), Ionospheric photoelectrons: Comparing Venus, Earth, Mars and Titan, *Planet. Space Sci.*, **59**(10), 1019–1027.
- Coates, A. J., et al. (2012), Cassini in Titan's tail: Caps observations of plasma escape, *J. Geophys. Res.*, **117**, A05324, doi:10.1029/2012JA017595.
- Coates, A. J., A. Wellbrock, R. Frahm, J. Winningham, A. Fedorov, S. Barabash, and R. Lundin (2015), Distant ionospheric photoelectron energy peak observations at Venus, *Planet. Space Sci.*, **113**, 378–384.
- Connerney, J., M. Acuña, N. Ness, G. Kletetschka, D. Mitchell, R. Lin, and H. Reme (2005), Tectonic implications of Mars crustal magnetism, *Proceedings of the national Academy of Sciences of the United States of America*, **102**(42), 14,970–14,975.
- Connerney, J., J. Espley, P. Lawton, S. Murphy, J. Odom, R. Oliverson, and D. Sheppard (2015), The MAVEN magnetic field investigation, *Space Sci. Rev.*, **195**, 257–291.
- Dong, C., S. W. Bougher, Y. Ma, G. Toth, A. F. Nagy, and D. Najib (2014), Solar wind interaction with Mars upper atmosphere: Results from the one-way coupling between the multifluid MHD model and the MTGCM model, *Geophys. Res. Lett.*, **41**, 2708–2715, doi:10.1002/2014GL059515.
- Dong, C., S. W. Bougher, Y. Ma, G. Toth, Y. Lee, A. F. Nagy, V. Tennishev, D. J. Pawlowski, M. R. Combi, and D. Najib (2015), Solar wind interaction with the Martian upper atmosphere: Crustal field orientation, solar cycle, and seasonal variations, *J. Geophys. Res. Space Physics*, **120**, 7857–7872, doi:10.1002/2015JA020990.
- Duru, F., D. Gurnett, D. Morgan, J. Winningham, R. Frahm, and A. Nagy (2011), Nightside ionosphere of Mars studied with local electron densities: A general overview and electron density depressions, *J. Geophys. Res.*, **116**, A10316, doi:10.1029/2011JA016835.
- Fillingim, M., L. Peticolas, R. Lillis, D. Brain, J. Halekas, D. Lummerzheim, and S. Bougher (2010), Localized ionization patches in the nighttime ionosphere of Mars and their electrodynamic consequences, *Icarus*, **206**(1), 112–119.
- Fillingim, M. O., L. M. Peticolas, R. J. Lillis, D. A. Brain, J. S. Halekas, D. L. Mitchell, R. P. Lin, D. Lummerzheim, S. W. Bougher, and D. L. Kirchner (2007), Model calculations of electron precipitation induced ionization patches on the nightside of Mars, *Geophys. Res. Lett.*, **34**, L12101, doi:10.1029/2007GL029986.
- Fox, J. L. (1993), The production and escape of nitrogen atoms on Mars, *J. Geophys. Res.*, **98**(E2), 3297–3310.
- Fox, J. L., J. F. Brannon, and H. S. Porter (1993), Upper limits to the nightside ionosphere of Mars, *Geophys. Res. Lett.*, **20**, 1339–1342, doi:10.1029/93GL01349.
- Frahm, R., et al. (2006), Carbon dioxide photoelectron energy peaks at Mars, *Icarus*, **182**(2), 371–382.
- Frahm, R., et al. (2010), Estimation of the escape of photoelectrons from Mars in 2004 liberated by the ionization of carbon dioxide and atomic oxygen, *Icarus*, **206**(1), 50–63.
- González-Galindo, F., J.-Y. Chaufray, M. López-Valverde, G. Gilli, F. Forget, F. Leblanc, R. Modolo, S. Hess, and M. Yagi (2013), Three-dimensional Martian ionosphere model: I. The photochemical ionosphere below 180 km, *J. Geophys. Res. Planets*, **118**, 2105–2123, doi:10.1002/jgre.20150.
- Gurnett, D. A., et al. (2008), An overview of radar soundings of the Martian ionosphere from the Mars Express spacecraft, *Adv. Space Res.*, **41**, 1335–1346, doi:10.1016/j.asr.2007.01.062.
- Haider, S. A., J. Kim, A. F. Nagy, C. N. Keller, M. I. Verigin, K. I. Gringauz, N. M. Shutte, K. Szego, and P. Kiraly (1992), Calculated ionization rates, ion densities, and airglow emission rates due to precipitating electrons in the nightside ionosphere of Mars, *J. Geophys. Res.*, **97**, 10,637–10,641, doi:10.1029/92JA00317.
- Harada, Y., et al. (2016), MAVEN observations of energy-time dispersed electron signatures in Martian crustal magnetic fields, *Geophys. Res. Lett.*, **43**, 939–944, doi:10.1002/2015GL067040.
- Harnett, E. M., and R. M. Winglee (2005), Three-dimensional fluid simulations of plasma asymmetries in the Martian magnetotail caused by the magnetic anomalies, *J. Geophys. Res.*, **110**, A07226, doi:10.1029/2003JA010315.
- Jakosky, B. M., et al. (2015), The Mars Atmosphere and Volatile Evolution (MAVEN) mission, *Space Sci. Rev.*, **195**(1–4), 3–48, doi:10.1007/s11214-015-0139-x.
- Liemohn, M. W., D. L. Mitchell, A. F. Nagy, J. L. Fox, T. W. Reimer, and Y. Ma (2003), Comparisons of electron fluxes measured in the crustal fields at Mars by the MGS magnetometer/electron reflectometer instrument with a B field-dependent transport code, *J. Geophys. Res.*, **108**(E12), 5134, doi:10.1029/2003JE00215.
- Liemohn, M. W., et al. (2006a), Numerical interpretation of high-altitude photoelectron observations, *Icarus*, **182**, 383–395, doi:10.1016/j.icarus.2005.10.036.
- Liemohn, M. W., Y. Ma, R. A. Frahm, X. Fang, J. U. Kozyra, A. F. Nagy, J. D. Winningham, J. R. Sharber, S. Barabash, and R. Lundin (2006b), Mars global MHD predictions of magnetic connectivity between the dayside ionosphere and the magnetospheric flanks, *Space Sci. Rev.*, **126**, 63–76, doi:10.1007/s11214-006-9116-8.
- Liemohn, M. W., Y. Ma, A. Nagy, J. Kozyra, J. Winningham, R. Frahm, J. Sharber, S. Barabash, and R. Lundin (2007), Numerical modeling of the magnetic topology near Mars auroral observations, *Geophys. Res. Lett.*, **34**, L24202, doi:10.1029/2007GL031806.
- Lillis, R. J., D. L. Mitchell, R. P. Lin, and M. H. Acuña (2008a), Electron reflectometry in the Martian atmosphere, *Icarus*, **194**(2), 544–561.
- Lillis, R. J., H. V. Frey, M. Manga, D. L. Mitchell, R. P. Lin, M. H. Acuña, and S. W. Bougher (2008b), *Icarus*, **194**(2), 575–596.
- Lillis, R. J., M. O. Fillingim, L. M. Peticolas, D. A. Brain, R. P. Lin, and S. W. Bougher (2009), Nightside ionosphere of Mars: Modeling the effects of crustal magnetic fields and electron pitch angle distributions on electron impact ionization, *J. Geophys. Res.*, **114**, E11009, doi:10.1029/2009JE003379.
- Ma, Y. J., X. Fang, A. F. Nagy, C. T. Russell, and G. Toth (2014), Martian ionospheric responses to dynamic pressure enhancements in the solar wind, *J. Geophys. Res. Space Physics*, **119**, 1272–1286, doi:10.1002/2013JA019402.
- Mantas, G. P., and W. B. Hanson (1979), Photoelectron fluxes in the Martian ionosphere, *J. Geophys. Res.*, **84**(A2), 369–385, doi:10.1029/JA084iA02p00369.
- McFadden, J., et al. (2015), MAVEN suprathermal and thermal ion composition (static) instrument, *Space Sci. Rev.*, **195**(1–4), 199–256.
- Mitchell, D., R. Lin, H. Reme, D. Crider, P. Cloutier, J. Connerney, M. Acuña, and N. Ness (2000), Oxygen auger electrons observed in Mars' ionosphere, *Geophys. Res. Lett.*, **27**(13), 1871–1874.
- Mitchell, D., R. Lin, C. Mazelle, H. Reme, P. Cloutier, J. Connerney, M. Acuña, and N. Ness (2001), Probing Mars' crustal magnetic field and ionosphere with the MGS electron reflectometer, *J. Geophys. Res.*, **106**(E10), 23,419–23,427.

- Mitchell, D., et al. (2016), The MAVEN solar wind electron analyzer, *Space Sci. Rev.*, 200(1–4), 495–528.
- Morschhauser, A., V. Lesur, and M. Grott (2014), A spherical harmonic model of the lithospheric magnetic field of Mars, *J. Geophys. Res. Planets*, 119, 1162–1188, doi:10.1002/2013JE004555.
- Najib, D., A. F. Nagy, G. Tóth, and Y. Ma (2011), Three-dimensional, multifluid, high spatial resolution MHD model studies of the solar wind interaction with Mars, *J. Geophys. Res.*, 116, A05204, doi:10.1029/2010JA016272.
- Némec, F., D. Morgan, D. Gurnett, and F. Duru (2010), Nightside ionosphere of Mars: Radar soundings by the Mars express spacecraft, *J. Geophys. Res.*, 115, E12009, doi:10.1029/2010JE003663.
- Seth, S. P., S. A. Haider, and K. I. Oyama (2002), Photoelectron flux and nightglow emissions of 5577 and 6300 Å due to solar wind electron precipitation in Martian atmosphere, *J. Geophys. Res.*, 107, 1324, doi:10.1029/2001JA000261.
- Sheehan, C. H., and J.-P. St-Maurice (2004), Dissociative recombination of N_2^+ , O_2^+ , and NO^+ : Rate coefficients for ground state and vibrationally excited ions, *J. Geophys. Res.*, 109, A03302, doi:10.1029/2003JA010132.
- Steckiewicz, M., et al. (2015), Altitude dependence of nightside Martian suprathermal electron depletions as revealed by MAVEN observations, *Geophys. Res. Lett.*, 42, 8877–8884, doi:10.1002/2015GL065257.
- Xu, S., and M. W. Liemohn (2015), Superthermal electron transport model for Mars, *Earth Space Sci.*, 2(3), 47–64, doi:10.1002/2014EA000043.
- Xu, S., M. W. Liemohn, and D. L. Mitchell (2014), Solar wind electron precipitation into the dayside Martian upper atmosphere through the cusps of strong crustal fields, *J. Geophys. Res. Space Physics*, 119, 10,100–10,115, doi:10.1002/2014JA020363.
- Xu, S., M. Liemohn, S. Bougher, and D. Mitchell (2015a), Enhanced carbon dioxide may explain the dust-storm-related increase in high-altitude photoelectron fluxes at Mars, *Geophys. Res. Lett.*, 42, 9702–9710, doi:10.1002/2015GL066043.
- Xu, S., M. W. Liemohn, W. Peterson, J. Fontenla, and P. Chamberlin (2015b), Comparison of different solar irradiance models for the superthermal electron transport model for Mars, *Planet. Space Sci.*, 119, 62–68, doi:10.1016/j.pss.2015.09.008.
- Xu, S., M. Liemohn, S. Bougher, and D. Mitchell (2016), Martian high-altitude photoelectrons independent of solar zenith angle, *J. Geophys. Res. Space Physics*, 3767–3780, doi:10.1002/2015JA022149.
- Zhang, M. H. G., J. G. Luhmann, and A. J. Kliore (1990), An observational study of the nightside ionospheres of Mars and Venus with radio occultation methods, *J. Geophys. Res.*, 95, 17,095–17,102, doi:10.1029/JA095iA10p17095.